

Supplementary material for: MARTINI Coarse Grained models of imidazolium-based ionic liquids: from nanostructural organization to liquid-liquid extraction

Luis Itza Vazquez-Salazar*, Michele Selle^{†*}, Alex H. de Vries,
Siewert J. Marrink[†] and Paulo C. T. Souza[†]

Groningen Biomolecular Sciences and Biotechnology Institute and Zernike Institute for Advanced Materials, University of Groningen, Nijenborgh 7, 9747 AG Groningen, The Netherlands

* L.I.V.S. and M.S. made equal contributions to this work.

[†]Deceased on July 29th, 2018

[†] Corresponding Authors E-mail: p.c.telles.de.souza@rug.nl (P.C.T.S)

E-mail: s.j.marrink@rug.nl (S.J.M.).

Content:

1. Supplementary Tables

Table S1. Structural parameters of the CG models for the ionic liquids.

Table S2. Size of simulation box and number of molecules for the systems studied.

Table S3. IL density as a function of temperature using PME.

Table S4. IL density as a function of temperature using Reaction Field.

2. Supplementary Figures

Figure S1. Density Vs Temperature for PME.

Figure S2. Number of carbons vs Density for PME.

Figure S3. Density Vs Temperature for Reaction Field.

Figure S4. Number of carbons vs Density for Reaction Field.

Figure S5. Experimental density vs CG density for Reaction Field.

Figure S6. Head-Head radial distribution function of the different IL's at 303 K.

Figure S7. Head-anion radial distribution function of the different IL's at 303 K.

Figure S8. Anion-anion radial distribution function of the different IL's at 303 K.

Figure S9. Nanodomain size with respect to the temperature.

Figure S10. Radial distribution functions of C12 as a function of temperature.

Figure S11. Diffusion plot of cation with respect to the temperature.

Figure S12. Diffusion plot of anion with respect to the temperature.

Figure S13. Viscosity with respect to the temperature.

Figure S14. Partial density profile of the system petroleum oil-C12.

Figure S15. Snapshots of the biphasic system petroleum oil-IL.

Figure S16. Potential of mean force of moving benzene or octane from the IL phase to the petroleum oil phase.

Figure S17. Snapshots of the biphasic system fish oil-IL.

Figure S18. Partial density profile of the system fish oil-C2 without octane.

Figure S19. Partial density profile of the system fish oil-C2 with octane.

Figure S20. Potential of mean force of moving DHA, PAL or OLE from the IL phase to the fish oil phase.

3. Supplementary Methods

3.1 Calculation of partial charges with quantum mechanics models.

3.2 Details of full atom simulation of IL.

4. Supplementary Video

5. Supplementary References

1. Supplementary Tables

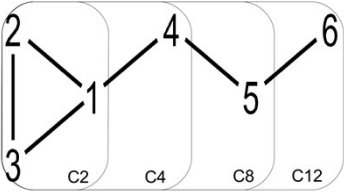
				
Ring constraints (nm)				
<i>ij</i>	C2	C4	C8	C12
1-2	0.285			
2-3	0.315			
1-3	0.285			
Bonds				
	C2	C4	C8	C12
<i>ij</i>	NA	1-4	1-4,4-5	1-4,4-5,5-6
Force Constant (kJ mol ⁻¹ nm ⁻²)	NA	7500	7500.0, 2500.0	7500.0,2500.0, 1250.0
Length(nm)	NA	0.312	0.312, 0.350	0.312,0.350,0.460
Angles				
	C2	C4	C8	C12
<i>ijk</i>	NA	3-1-4, 2-1-4	3-1-4, 2-1-4, 1-4-5	3-1-4,2-1-4,4-5-6
Angle	NA	120.0,120.0	120.0,120.0,180.0	120.0,120.0,180.0
Force Constant(kJ mol ⁻¹)	NA	50.0,50.0	50.0,50.0,25.0	50.0,50.0,25.0
Dihedrals				
	C2	C4	C8	C12
<i>ijkl</i>	NA	4-2-3-1		
Angle	NA	0		
Force Constant (kJ mol ⁻¹)	NA	200		

Table S1. Structural parameters of the CG models for the ionic liquids studied in this work.

Pure IL				
Cation	C2	C4	C8	C12
Size of box(nm)	6.4 x 6.4 x 6.4			
Molecules of Ionic liquid	600	600	600	565
Number of Particles	2400	3000	3600	3955
Petroleum Oil				
Cation	C2	C4	C8	C12
Size of box(nm)	5x5x9.5	5x5x10.6	5x5x12.4	5x5x14.2
IL Molecules	450			
Octane Molecules	450			
Benzene Molecules	73			
Number of Particles	2919	3369	3819	4269
Fish Oil				
Cation	C2	C4	C8	C12
Size of box(nm)	5x5x13 (5x5x17.2)	5x5x12.4 (5x5x17)	5x5x12.2 (5x5x16.7)	5x5x12.3 (5x5x16.7)
IL Molecules	477	371	265	216
DHA Molecules	12			
PAL Molecules	162			
OLE Molecules	162			
Octane Molecules*	463			
Number of Particles	3600(4526)	3547(4473)	3282(4208)	3204(4130)

Table S2. Size of simulation box and number of molecules for the systems simulated on this work. In the case of the fish oil between brackets are the values of the system for the case when octane is added to the simulation box. *Note:* Oleic Acid (OLE), Palmitic Acid (PAL), Docosahexaenoic Acid (DHA).

Temperature (K)	C2	C4	C8	C12
	Density (kg/m ³)	Density (kg/m ³)	Density (kg/m ³)	Density (kg/m ³)
293.15	1290.38	1192.76	1123.46	1079.08
303.15	1277.73	1181.28	1111.47	1069.92
313.15	1265.16	1169.61	1098.99	1057.30
323.15	1252.45	1158.02	1086.75	1043.92
333.15	1239.53	1146.05	1074.43	1028.32
343.15	1226.48	1134.22	1061.74	1015.92
353.15	1213.45	1122.39	1049.52	1003.85
363.15	1200.19	1110.19	1036.94	991.71
373.15	1186.95	1097.94	1024.52	979.62
383.15	1173.25	1085.46	1012.12	967.19
393.15	1159.35	1072.76	999.34	954.99

Table S3. Density vs Temperature for pure IL using PME.

Temperature (K)	C2	C4	C8	C12
	Density (kg/m ³)	Density (kg/m ³)	Density (kg/m ³)	Density (kg/m ³)
293.15	1288.76	1192.01	1123.79	1080.69
303.15	1276.24	1180.48	1112.01	1069.72
313.15	1263.65	1169.00	1099.63	1059.10
323.15	1251.15	1157.36	1087.51	1046.61
333.15	1238.40	1145.69	1075.08	1030.04
343.15	1225.45	1133.90	1062.80	1017.96
353.15	1212.39	1121.98	1050.09	1005.27
363.15	1199.31	1109.83	1037.83	992.86
373.15	1186.06	1097.75	1025.24	980.75
383.15	1172.50	1085.39	1012.54	968.37
393.15	1159.05	1072.80	999.83	955.76

Table S4. Density vs Temperature for pure IL using Reaction Field

2. Supplementary Figures

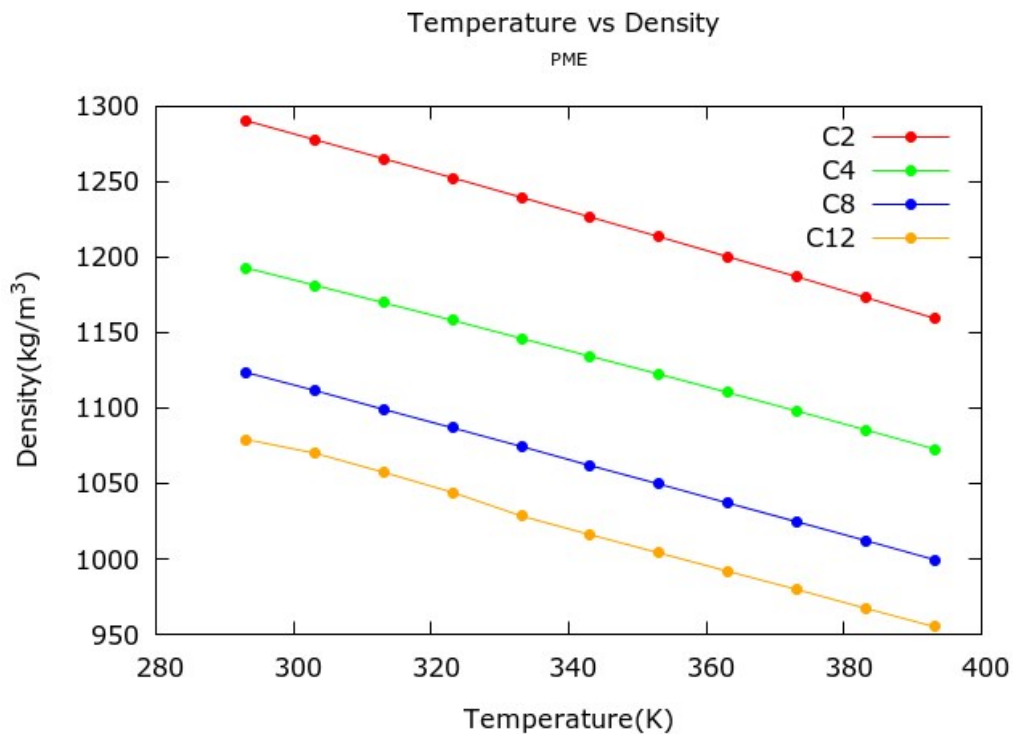


Figure S1. Profile of Density Vs Temperature for PME

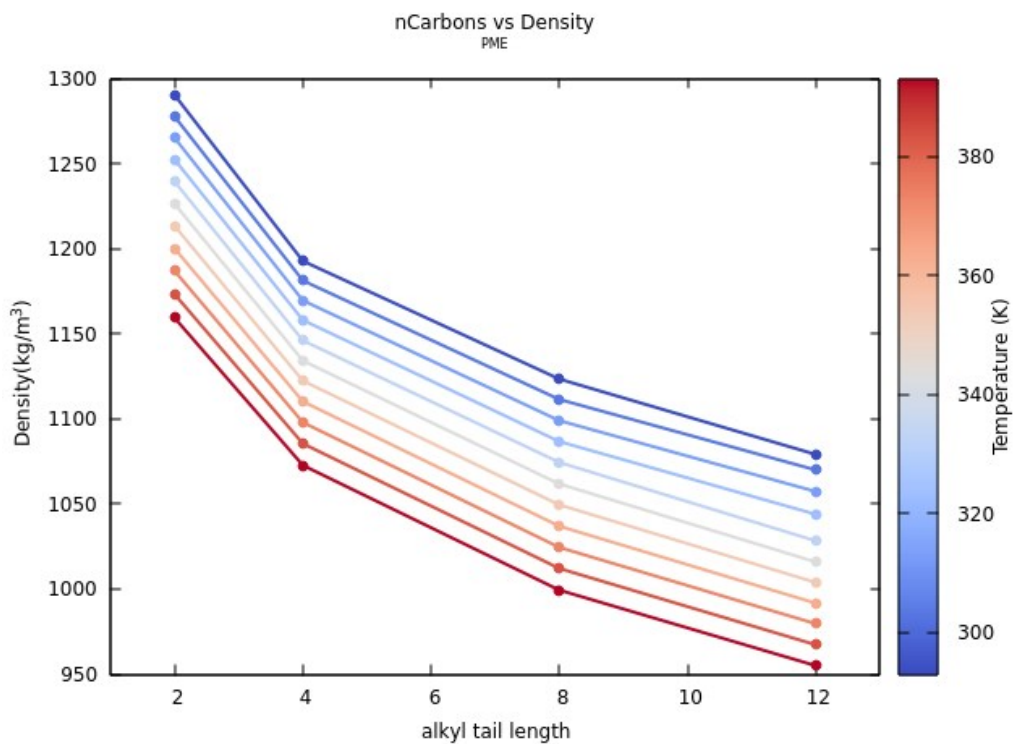


Figure S2. Profile of number of carbons vs Density for PME

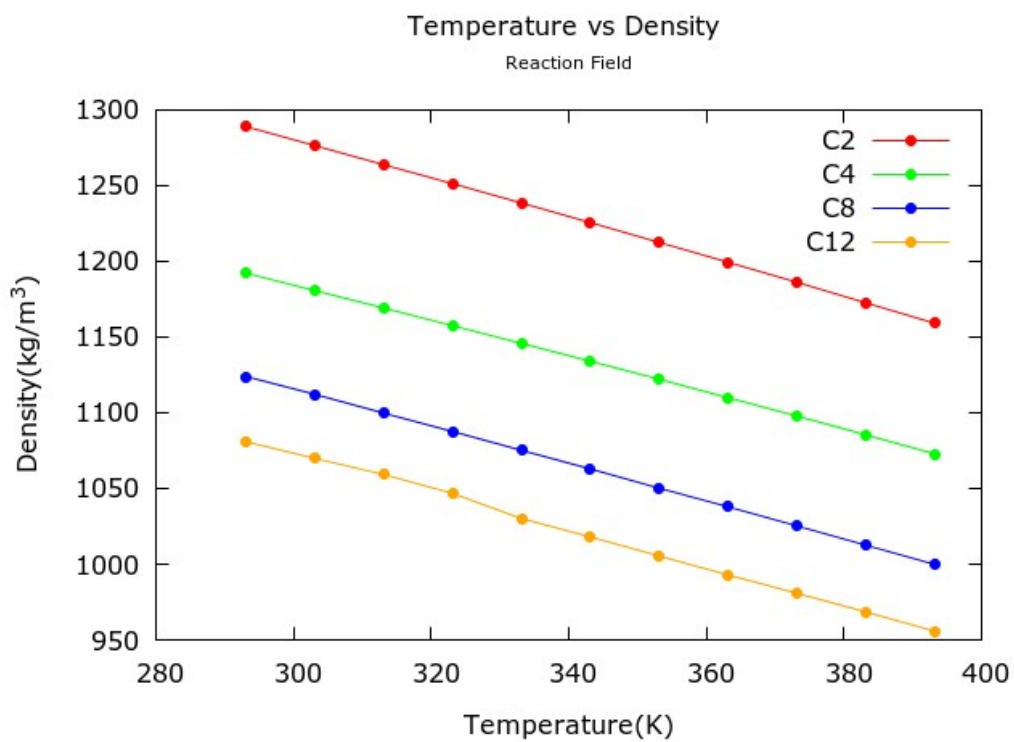


Figure S3. Profile of Temperature Vs density with Reaction Field

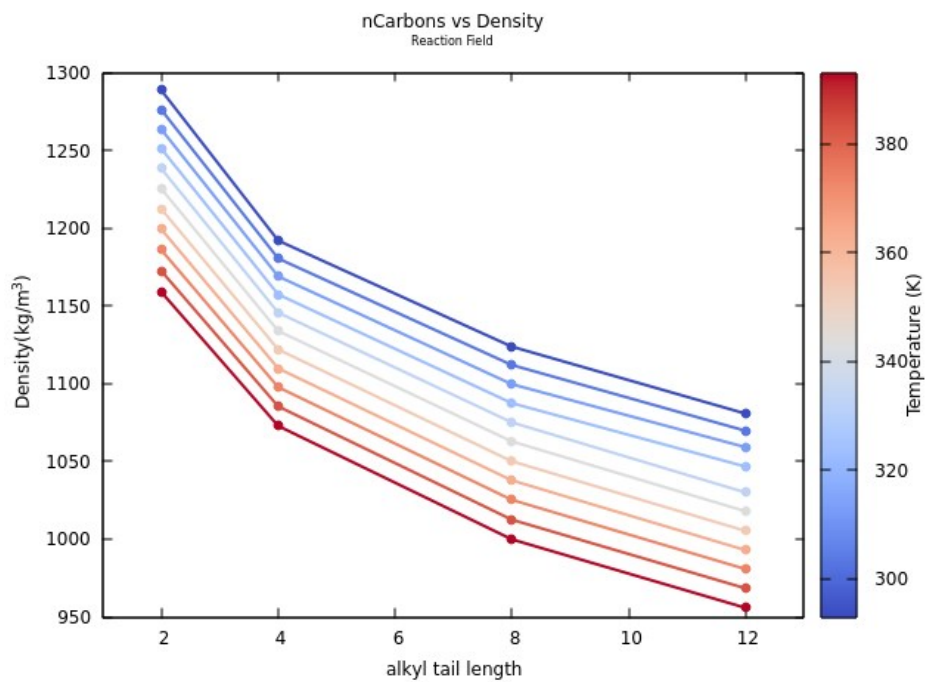


Figure S4. Profile of number of Carbons vs Density for Reaction Field.

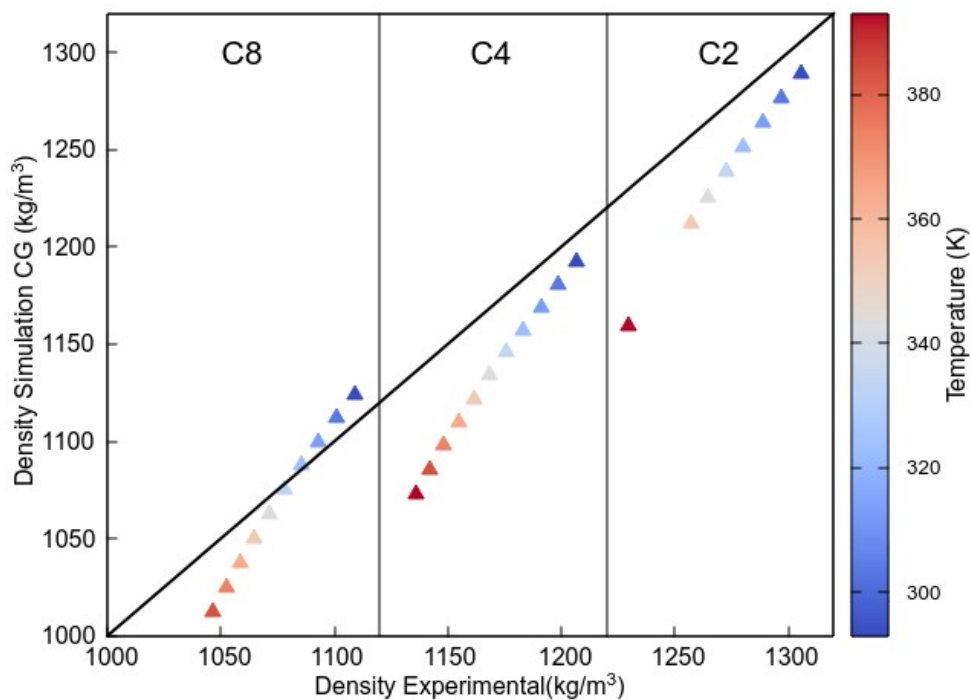


Figure S5. Experimental vs CG density for reaction field method.

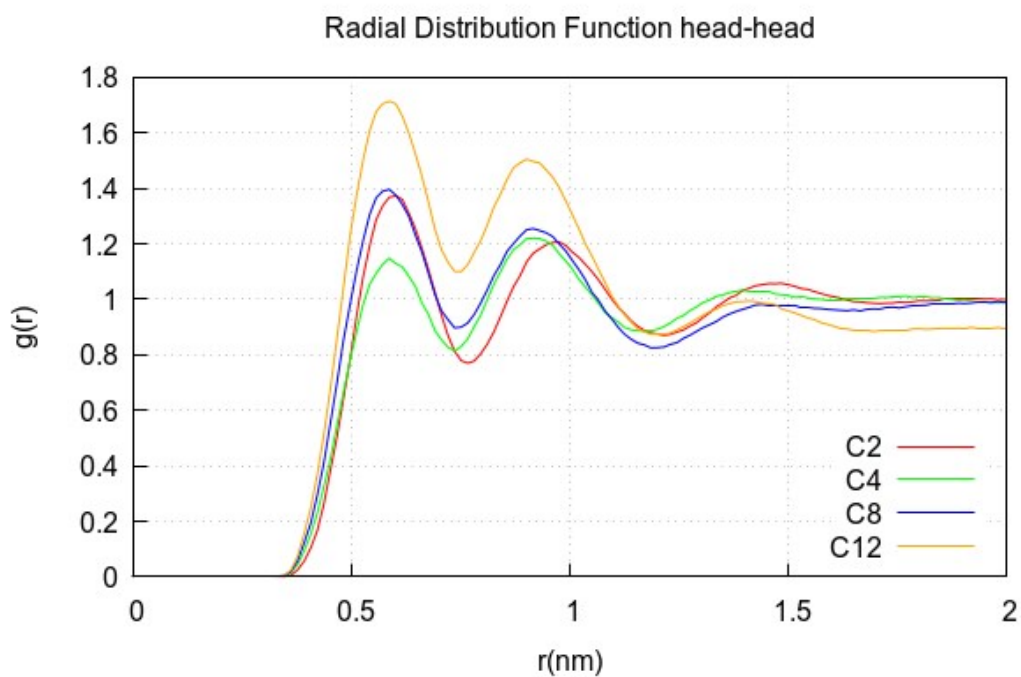


Figure S6. Imidazolium ring-Imidazolium ring radial distribution function of the different IL's at 303 K studied on this work.

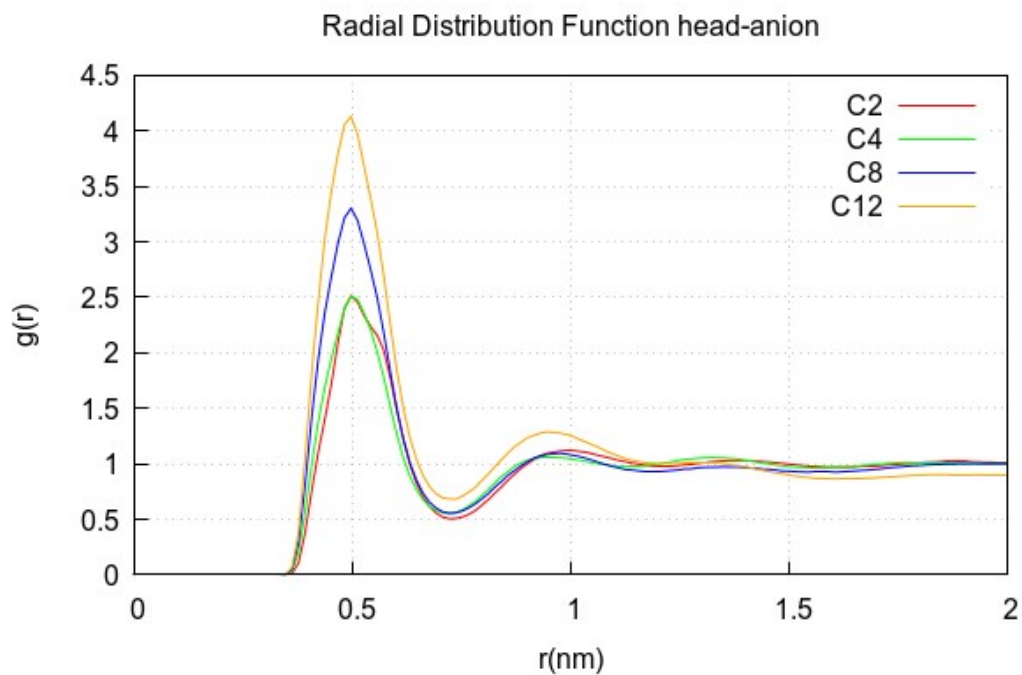


Figure S7. Imidazolium ring-anion radial distribution function of the different IL's at 303 K studied on this work.

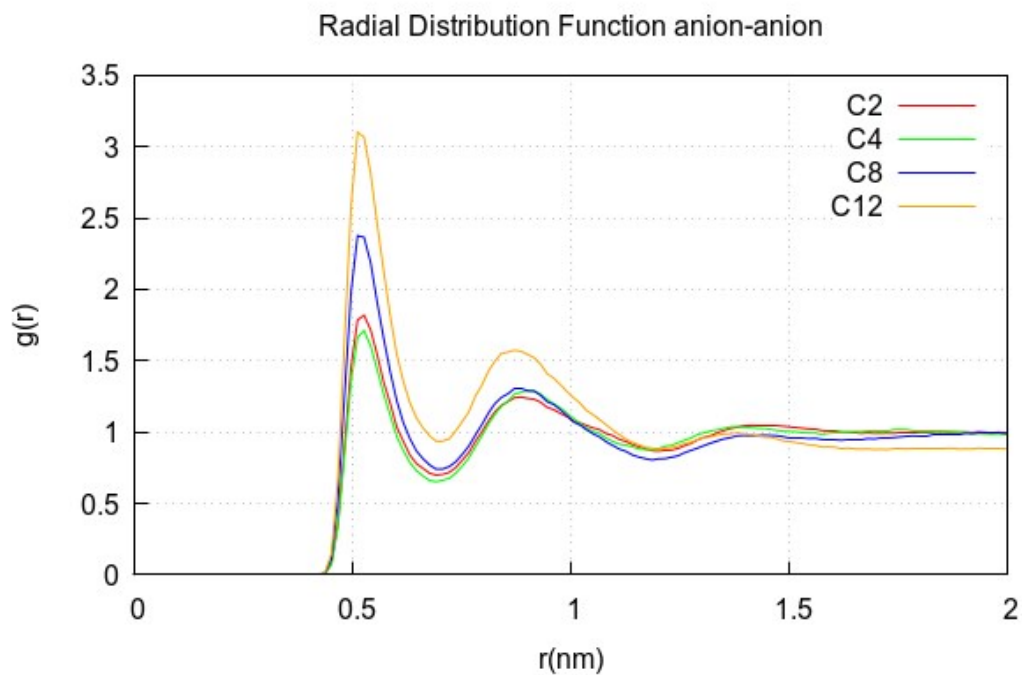


Figure S8. Anion-anion radial distribution function of the different IL's at 303 K studied on this work.

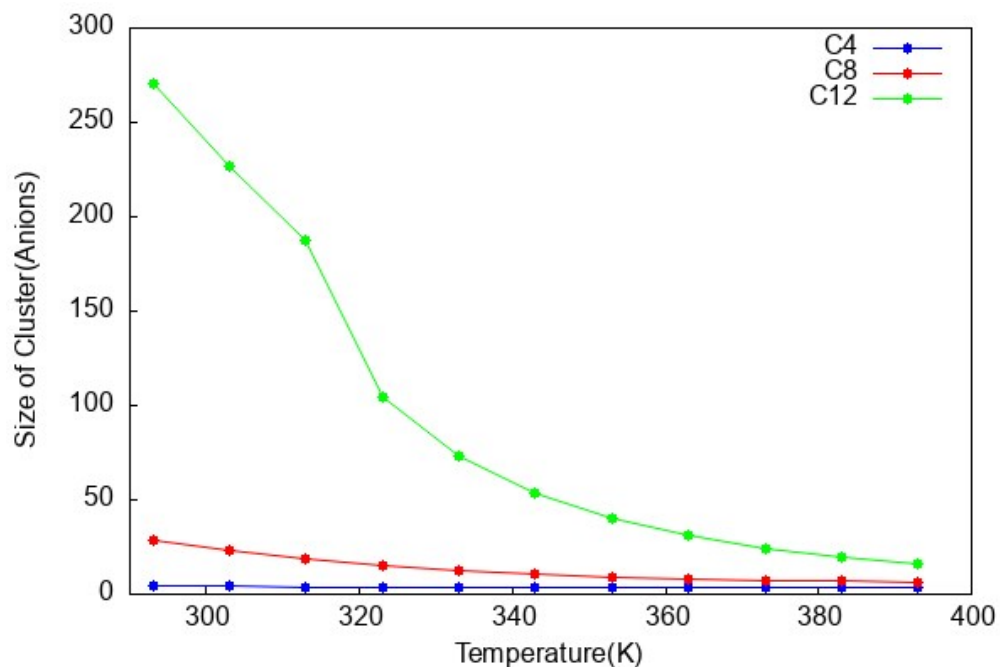


Figure S9. Nanodomain size with respect to the temperature.

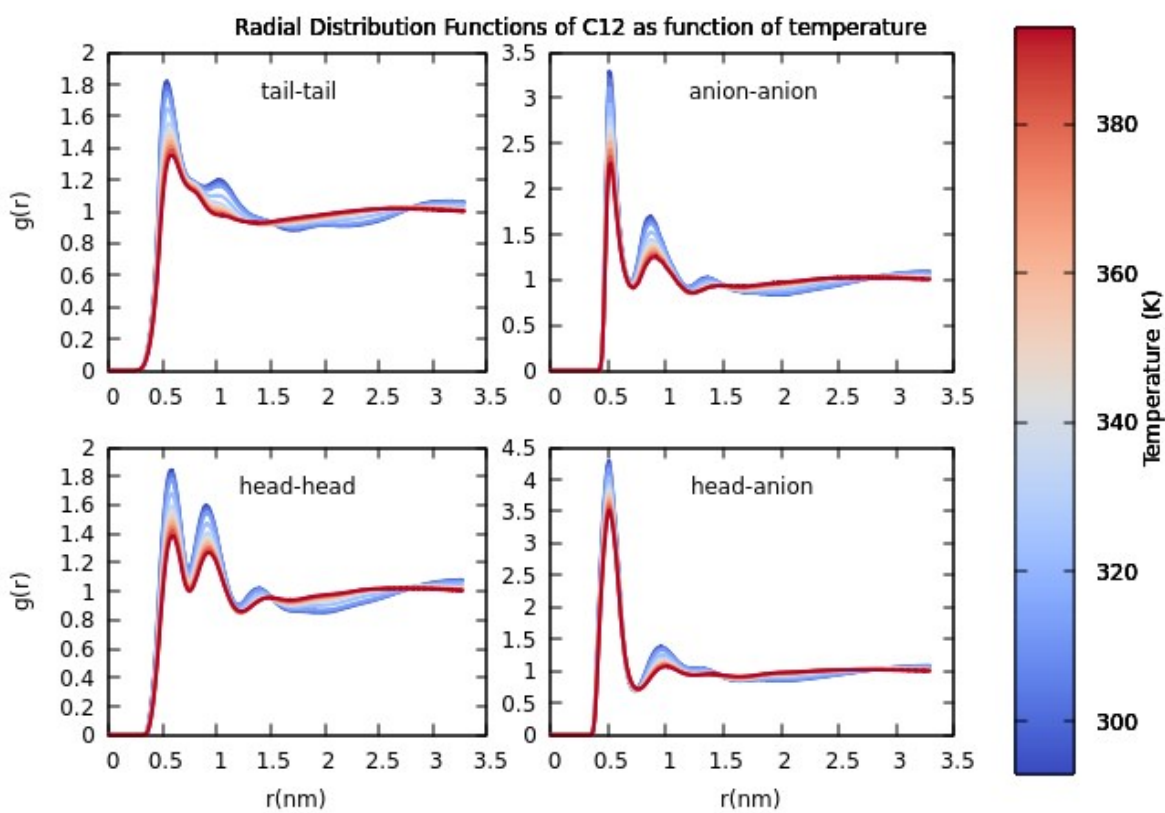


Figure S10. Radial distribution function of C12 as a function of temperature.

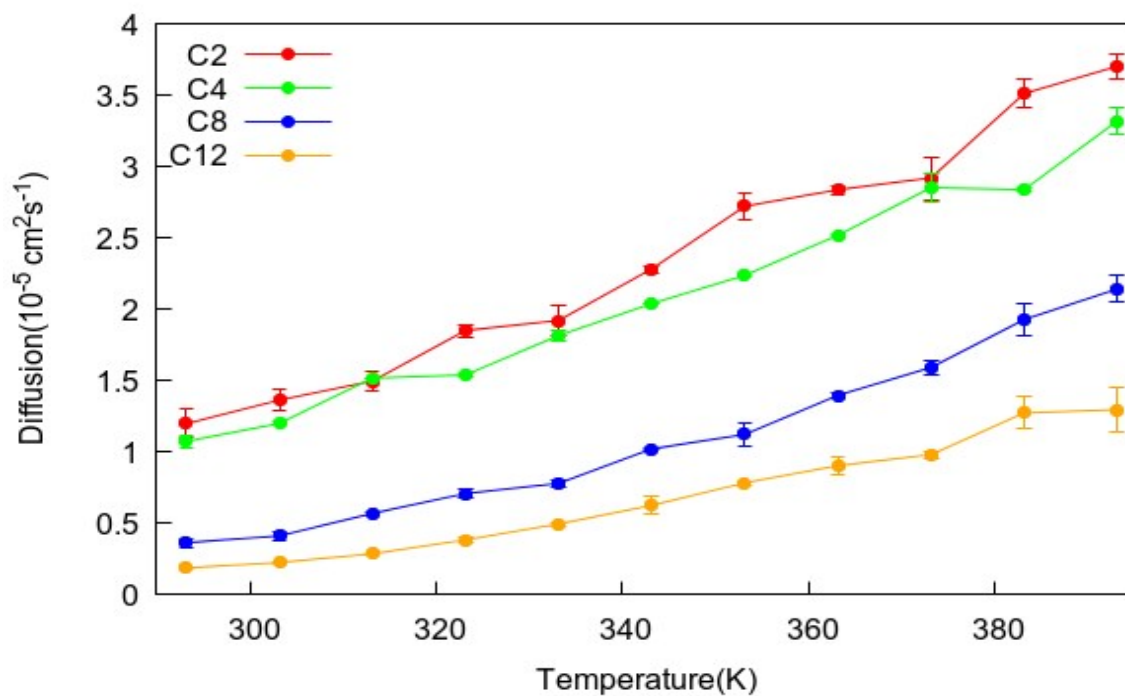


Figure S11. Diffusion of cation with respect to the temperature.

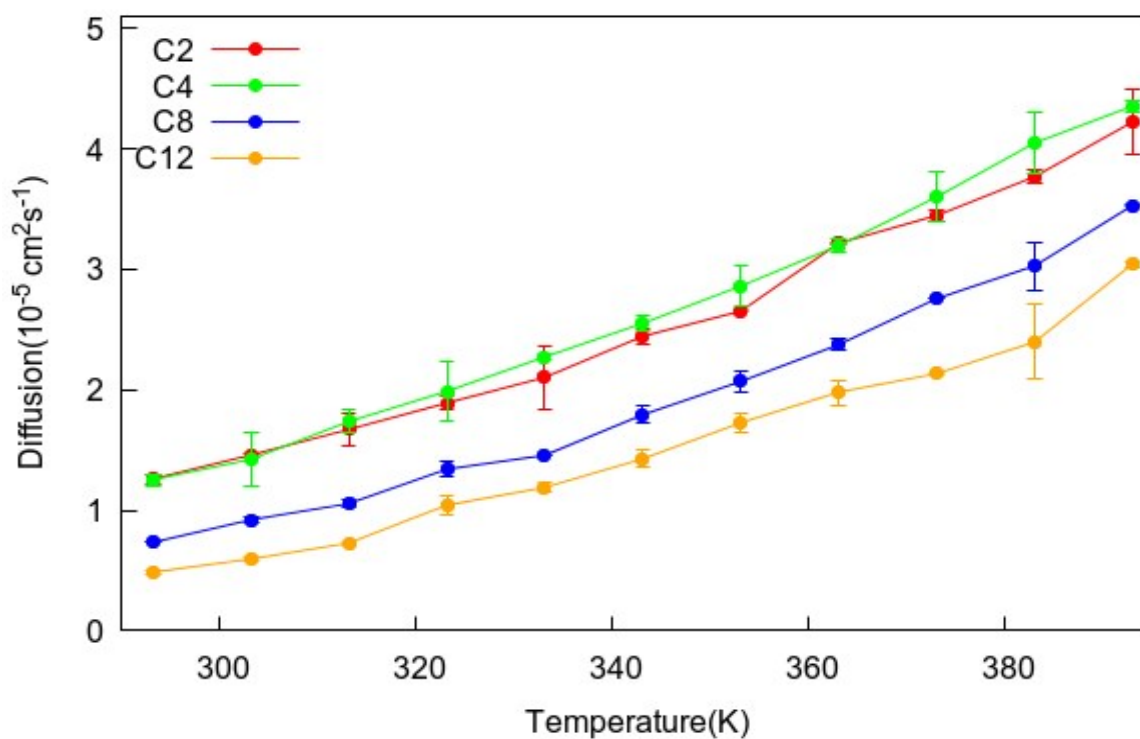


Figure S12. Diffusion of the anion with respect to the temperature.

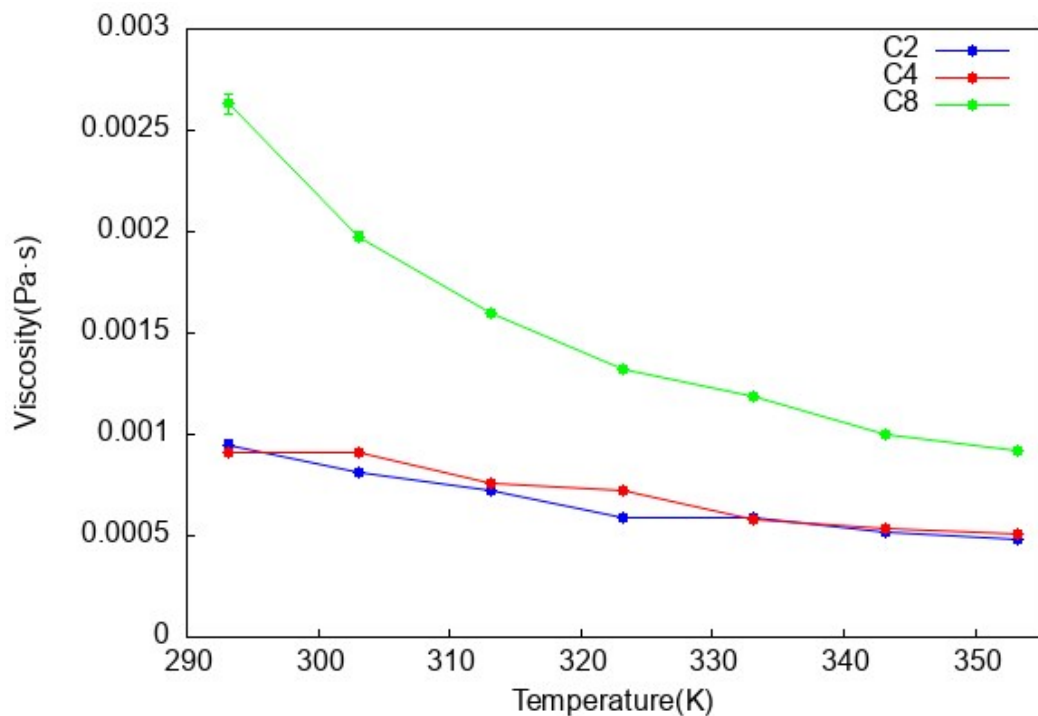


Figure S13. Profile of viscosity vs Temperature for the different ionic liquids evaluated on this work. Only ionic liquids based on $[C_2mim]^+$, $[C_4mim]$ and $[C_8mim]$ cations were considered, as experimental data for comparison is available for them.

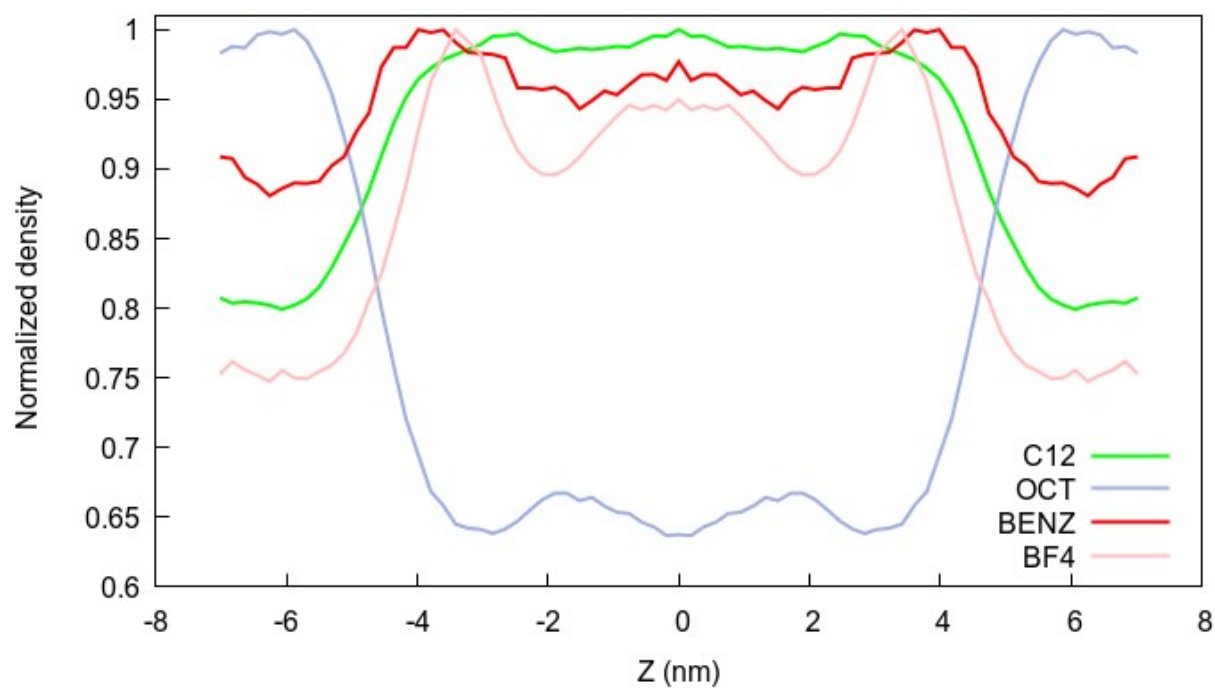


Figure S14. Partial density profile of the system petroleum oil-IL for the cation C12.

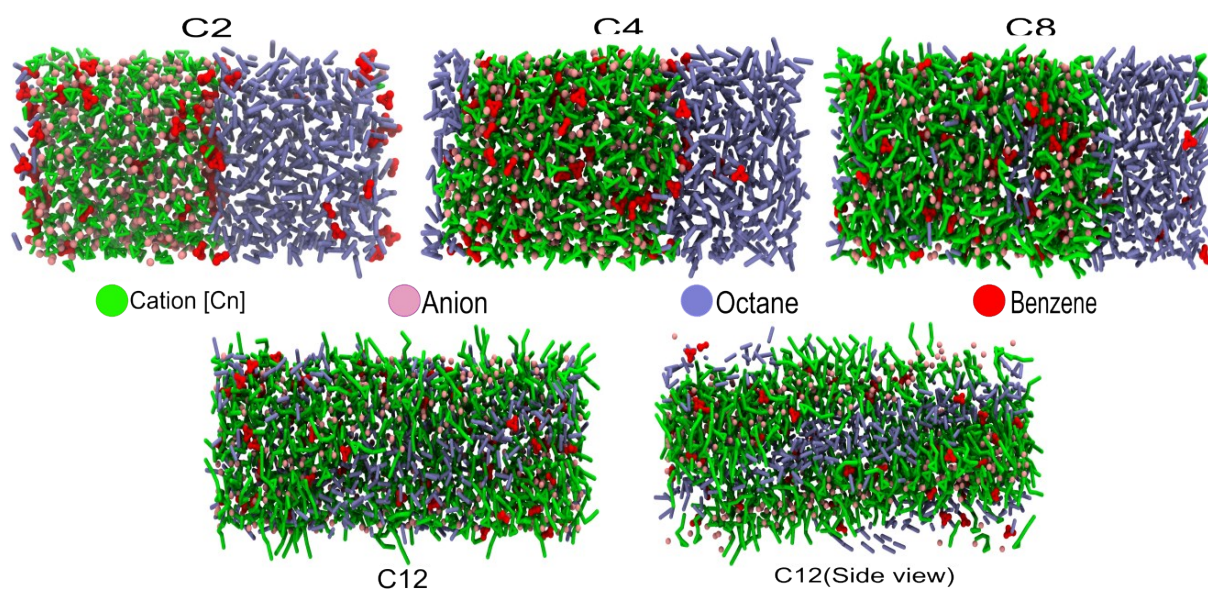


Figure S15. Snapshots of the final state of the simulation boxes for the system IL-octane-benzene. Colour code: In green, the cation composed for the imidazolium ring and the alkyl tail. In pink, the beads correspond to the anion. In violet, the octane molecules and in red, the molecules of benzene.

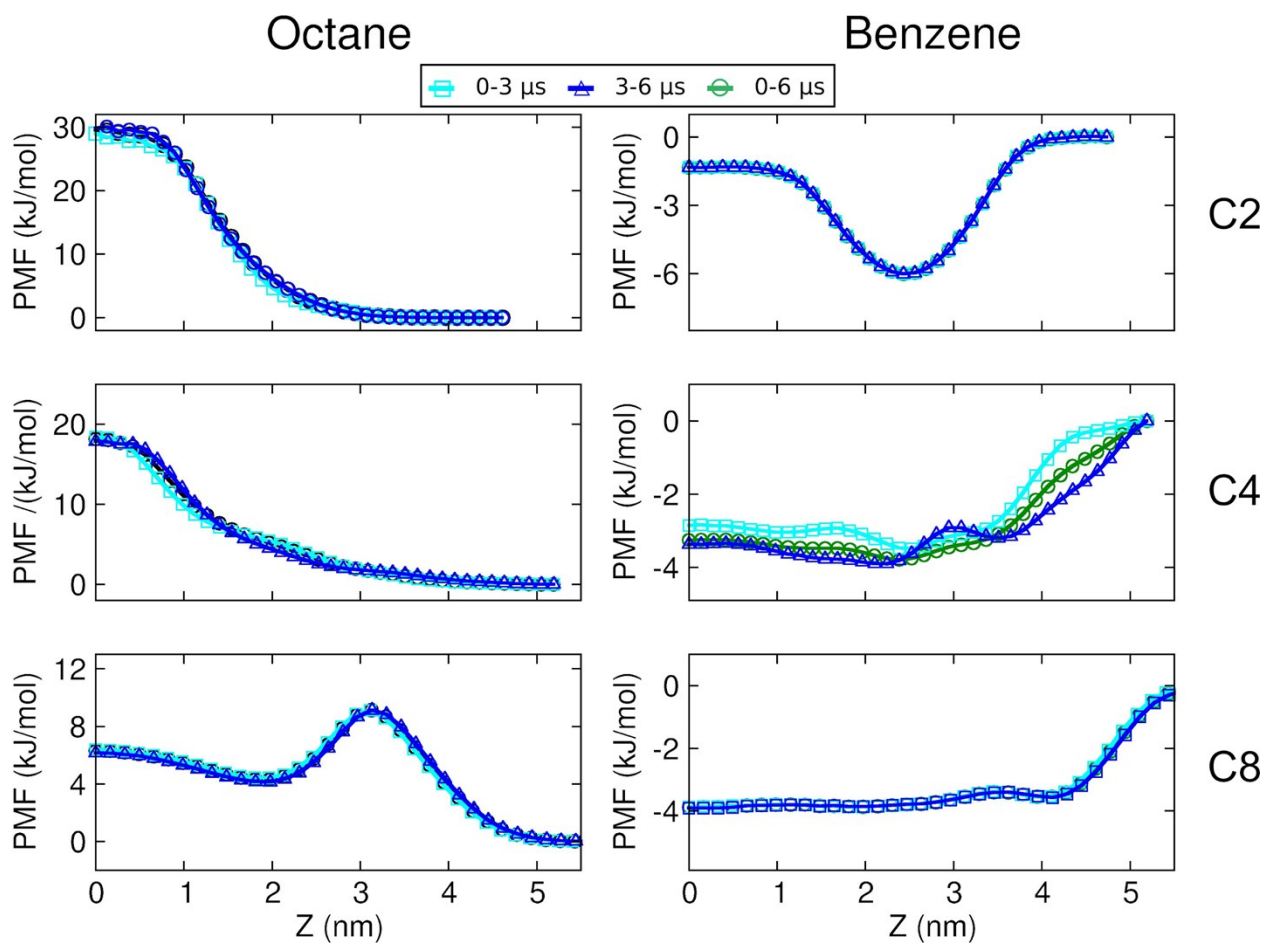


Figure S16. Potential of mean force of moving benzene or octane from the IL phase (bulk liquid at Z equal to 0) to the petroleum oil phase (maximum Z value, around 5-6 nm depending on the system). For comparison, all PMFs were shifted to zero at the petroleum oil phase. From the top to the bottom plots, we showed the PMFs using C2 (top), C4 (middle) and C8 (bottom) ionic liquids. Plots on the left are for the benzene PMFs while the plots on the right are for the octane PMFs. The convergence was checked using block averaging, with the plots showing PMFs obtained with the whole sampling (0-6 μ s, green line and circle points) and with first (0-3 μ s, cyan line and square points) and last (3-6 μ s, blue line and triangles) of the trajectories.

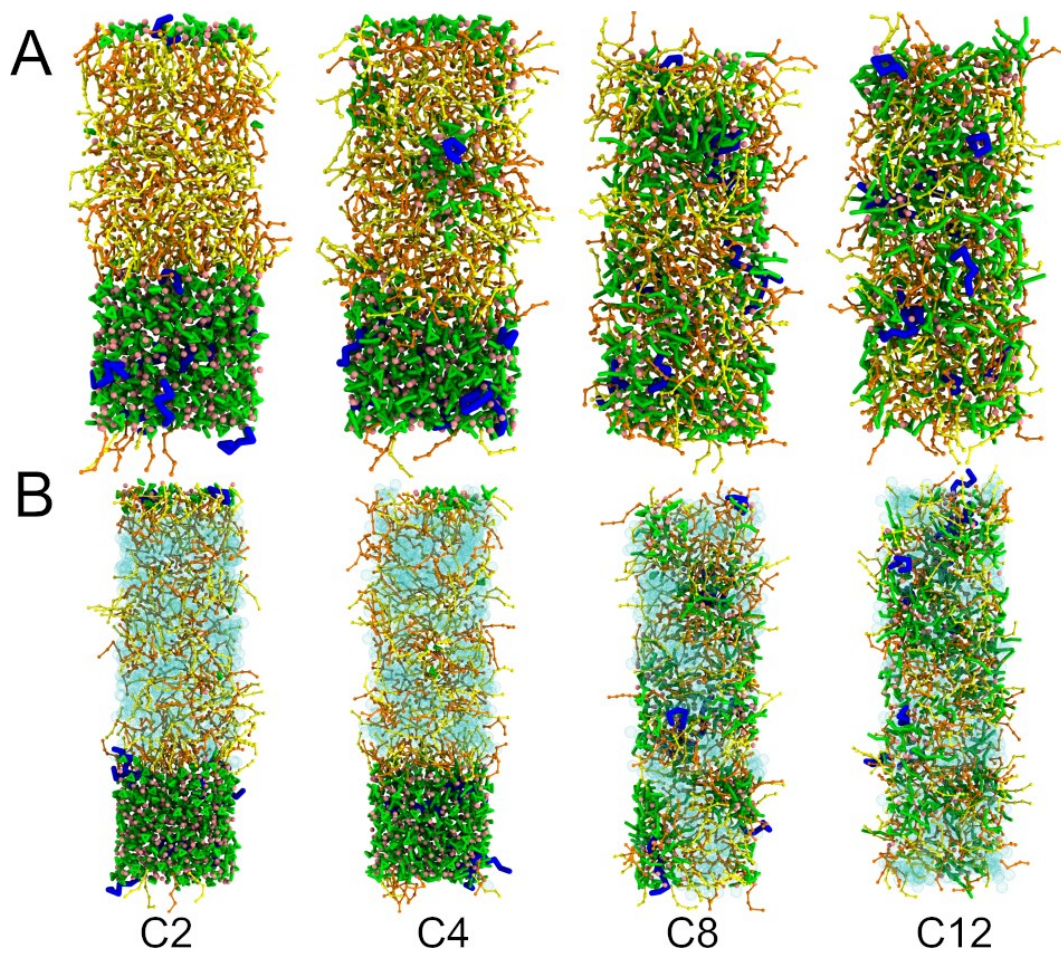


Figure S17. Snapshots of the final simulation box of the ILs and the fish oil without (A) and with (B) octane. Colour code: In green, the cation composed for the imidazolium ring and the alkyl tail. In pink, the beads correspond to the anion. For the fatty acids, DHA is shown in blue, OLE and PAL in yellow and orange, respectively. Octane is depicted in cyan.

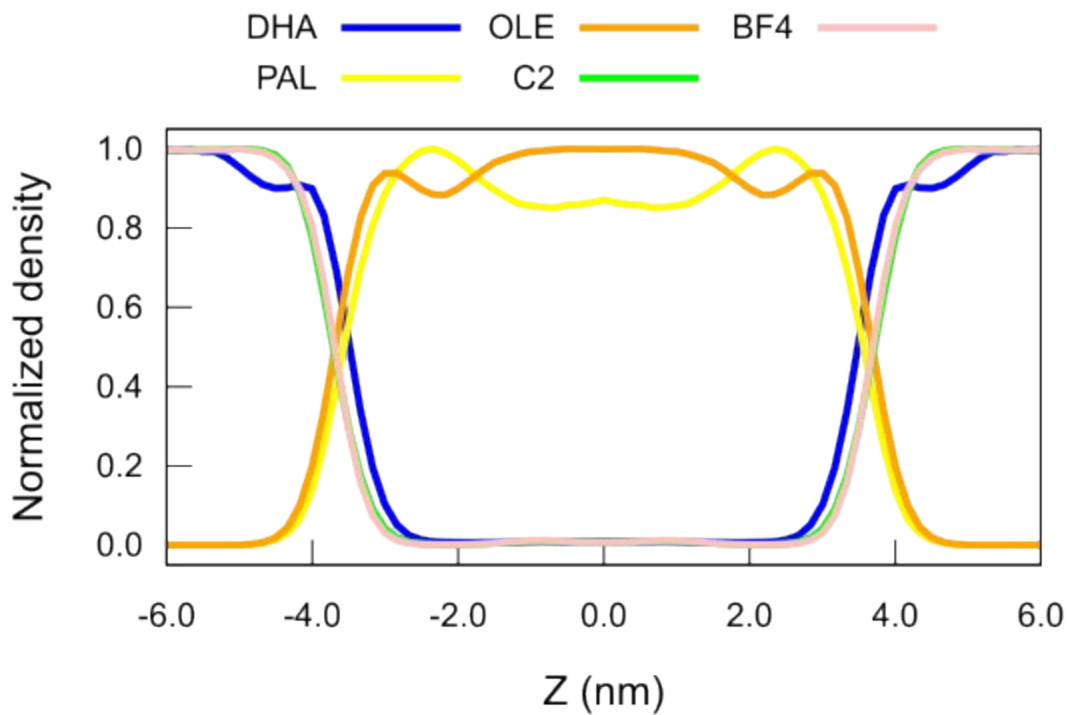


Figure S18. Partial density profile of the system fish oil-IL without octane for the cation C2

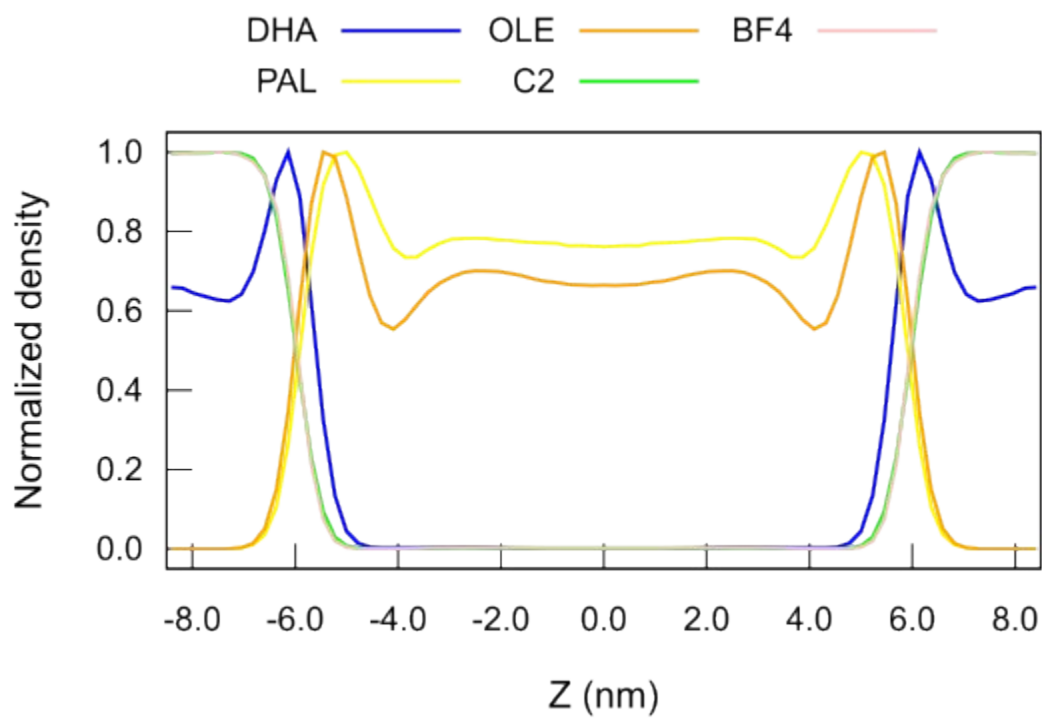


Figure S19. Partial density profile of the system fish oil-IL with octane for the cation C2

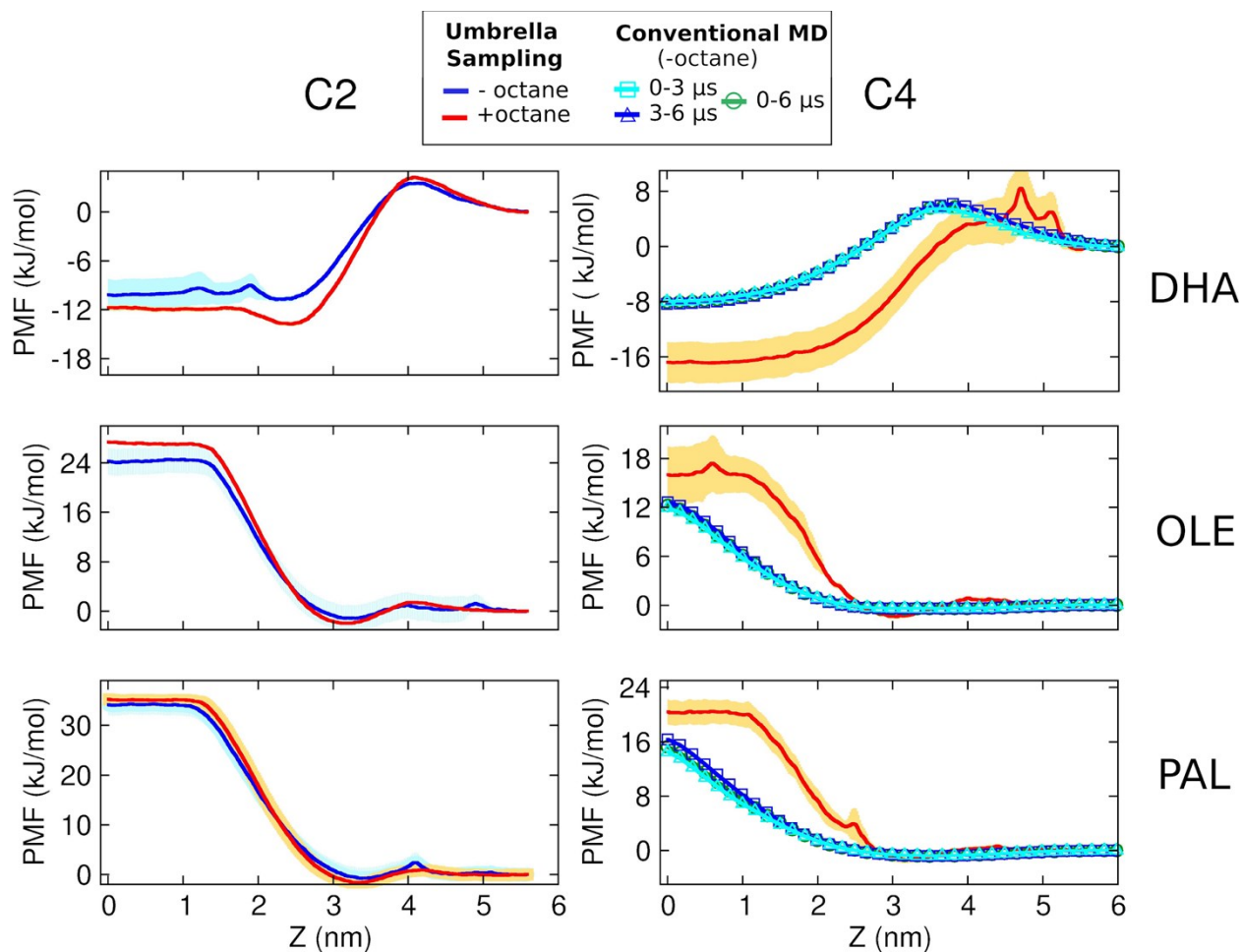


Figure S20. Potential of mean force of moving DHA, PAL or OLE from the IL phase (bulk liquid at Z equal to 0) to the fish oil phase (maximum Z value, around 5-6 nm depending on the system). For comparison, all PMFs were shifted to zero at the fish oil phase. From the top to the bottom plots, we showed the PMFs of DHA (top), OLE (middle) and PAL (bottom). Plots on the left are for the C2/fish oil system while the plots on the right are for the C4/fish oil system. For the umbrella sampling calculations, we show the converged PMFs (bold line) combined with error bars (area with light colors around the average), estimated with bootstrapping, for all biphasic systems with (red) and without (blue) the co-solvent octane, except C4 without octane. In this exceptional case, the PMF was directly estimated with conventional MD simulations, as performed for petroleum oil extractions (Figure S16). The convergence in this case is checked using block averaging, with the PMFs obtained with the whole sampling (0-6 μ s, green line and circle points) and with first (0-3 μ s, cyan line and square points) and last (3-6 μ s, blue line and triangles) of the trajectories.

3. Supplementary Methods

3.1 Calculation of partial charges with quantum mechanics models.

We have constructed effective charges for the MARTINI model by redistributing the distributed partial charges and dipoles calculated by quantum-chemistry over the atomic centers in a manner that preserves the local dipole moments optimally, akin to the Dipole Preserving Charge (DPC) introduced by Thole and van Duijnen¹. The analysis as implemented here, aims to represent the charge and dipole distribution of the full atomistic model by placing partial charges on all beads of the coarse-grained model. The partial charges obey the restraints (common in many charge-fitting schemes such as RESP²) that the total charge is conserved and that the total dipole moment is conserved, but in addition, weight factors are introduced that favor placing the partial charges on the beads nearest to the atom that bears the local charge and dipole. This idea is taken from the DPC analysis; the weighting scheme is exponential, i.e. the weight decreases exponentially with the distance of the bead to the atom. The scheme is implemented in a *Mathematica*³ NOTEBOOK as a matrix inversion problem. The scheme can take any set of charges and dipoles (and can be extended to higher-order multipoles). In this study, the distributed charges and dipoles of the atomistic model were obtained by performing a Distributed Multipole Analysis (DMA) due to Stone⁴ on the quantum-chemical charge density of the optimized geometry of an imidazolium cation in vacuum, as implemented in GAMESS-UK.⁵ The optimization and charge density calculation were done at the Density Functional Theory (DFT) level using the 6-31G* basis set and the PBE0 functional. The sensitivity of the resulting partial charges on the beads to the decay parameter of the exponential weighting was tested and found to be small in the range of a decay length of 5-20 Angstrom. The partial charges were calculated for MeMelm, MeEtlm, and EtEtlm. The partial charges for longer chains are the same as for the EtEtlm. The final partial charges as used in the simulations are shown in Figure 1 in the main text.

3.2 Details of the all-atom MD simulations

Simulations were performed using the force field designed for Canongia-Lopes and Padua^{6,7} which is extensively used in the literature for the study of ILs. The systems for C2, C4 and C8 were built with 250 pairs with the aid of the FFTool⁸ and the Packmol software⁹. The systems were minimized at 1 K for 10000 steps and a second time at 303 K for the same number of steps. Equilibration period was 300 ps with a time step of 1 fs. The production was run for 100 ns with a time step of 2 fs. In equilibration and production, we use the v-scale thermostat¹⁰ with a coupling time of 0.1 ps. The pressure was controlled with the Parrinello-Rahman barostat¹¹. (compressibility 4.5×10^{-5} bar⁻¹) at 1 bar. We use PME for the electrostatic interactions with a cutoff of 1.6 nm. The rest of the settings were taken from Voroshilova and Chaban¹²

4. Supplementary Video

An extraction simulation of DHA (blue) from the fish oil model (PAL in yellow, and OLE in orange) using C4 IL ([C₄mim]⁺ in green and [BF₄]⁻ in pink). Octane (cyan) was added as co-solvent to the fish oil mixture. After equilibration, most of the DHA molecules are still in the fish oil phase. By the end of the movie (around 0.5 μ s) all DHA molecules already migrate to the IL phase. DHA molecules stay in the IL phase until the end of the 4.4 μ s trajectory.

5. Supplementary References

- 1 B. T. Thole and P. T. Duijnen, *Theoretica Chimica Acta*, 1983, 63, 209–221.
- 2 C. I. Bayly, P. Cieplak, W. Cornell and P. A. Kollman, *The Journal of Physical Chemistry*, 1993, 97, 10269–10280.
- 3 R. Walker, S. Wolfram and Wolfram Research, *The Mathematical Gazette*, 1989, 73, 363.
- 4 A. J. Stone, *Chemical Physics Letters*, 1981, 83, 233–239.
- 5 M. F. Guest, I. J. Bush, H. J. J. Van Dam, P. Sherwood, J. M. H. Thomas, J. H. Van Lenthe, R. W. A. Havenith and J. Kendrick, *Molecular Physics*, 2005, 103, 719–747.
- 6 J. N. C. Lopes, J. N. Canongia Lopes, J. Deschamps and A. A. H. Pádua, *The Journal of Physical Chemistry B*, 2004, 108, 11250–11250.
- 7 J. N. Canongia Lopes and A. A. H. Padua, *J. Phys. Chem. B*, 2006, **110**, 19586–19592.
- 8 A. Padua, FFTool, <https://github.com/agiliopadua/fftool>.
- 9 L. Martínez, R. Andrade, E. G. Birgin and J. M. Martínez, *J. Comput. Chem.*, 2009, **30**, 2157–2164.
- 10 G. Bussi, D. Donadio and M. Parrinello, *J. Chem. Phys.*, 2007, **126**, 014101.
- 11 M. Parrinello and A. Rahman, *Journal of Applied Physics*, 1981, 52, 7182–7190.
- 12 I. V. Voroshylova and V. V. Chaban, *J. Phys. Chem. B*, 2014, **118**, 10716–10724.